Journal of Power Sources 184 (2008) 23–28

Contents lists available at ScienceDirect

Journal of Power Sources

journal homepage: www.elsevier.com/locate/jpowsour

An original laboratory X-ray diffraction method for *in situ* investigations on the water dynamics in a fuel cell proton exchange membrane

A. Isopo*, V. Rossi Albertini

Istituto di Struttura della Materia, Consiglio Nazionale delle Ricerche (CNR), Via del fosso del cavaliere 100, 00133 Roma, Italy

ARTICLE INFO

Article history:
Received 15 January 2008
Received in revised form 30 May 2008
Accepted 8 June 2008
Available online 25 June 2008

Keywords:
Proton exchange membrane
Real-time X-ray diffraction
Water dynamics

ABSTRACT

A key issue of the polymer membrane-based fuel cells is the water management, since the polymeric electrolyte acts as a good protonic conductor only if sufficiently hydrated. Although models and theoretical studies are widely reported in the literature, experimental investigations are much less available, due to inherent difficulties to sample the membrane *in situ*. Among the techniques utilized for this purpose, the synchrotron radiation X-ray diffraction has been demonstrated to be a suitable tool to observe the real-time water dynamics in the polymeric membranes. To export this method in laboratories would represent a big advantage because of the limited access to synchrotron facilities. Clearly, the main problem in performing such studies by using conventional X-ray tubes consists of their much lower photon flux, particularly relevant when non-crystalline samples, as polymers, are to be investigated and when extreme collimations of the X-ray beams are required, as in the case of thin membranes.

In the present work, we propose a X-ray method, based on the energy dispersive X-ray diffraction, capable to overcome these drawbacks.

1. Introduction

Proton exchange membrane fuel cells (PEMFCs) can be regarded as possible candidates for the next-generation power sources, being very efficient in converting chemical into electrical energy and, at the same time, environmental friendly. The perfluorinated ionomer materials are, at present, the most promising for PEMFC applications; among them, Nafion® meets various remarkable requirements [1], such as high proton conductivity (when properly hydrated), high mechanical, thermal and chemical stability.

The exact mechanism of proton transport through Nafion membrane is still under debate, but it is generally accepted that the protons travel through the hydrophylic domains [2–4]. Therefore, proton conductivity is related to membrane hydration degree.

The water distribution across the membrane thickness is due to a number of competing phenomena, the main being the electro-osmotic drag [5,6] from the anode to the cathode and the water back-diffusion [7] in the opposite direction. Along with these, other effects inducing the membrane dehydration (membrane heating due to cell working, flux of the reactant gases, striction exerted by the FC graphite blocks on the membrane), as well as humidification of the reactant gases carried out to counterbalance such dehydration, are to be taken into account. As a result, to provide a realistic description of the actual water distribution inside the membrane by means of theoretical models [8–11] is not an easy task to solve, even in steady operating conditions.

Therefore, direct experimental investigations are indispensable for an accurate description of the water management and to possibly improve the cell performances. However, the difficulties in probing the water distribution across the membrane *in situ* restricts the range of techniques usable for this purpose and, consequently, the quantity of experimental data available in the literature.

The techniques utilized up to now are neutron imaging [12–14], small angle neutron scattering (SANS) [15], nuclear magnetic resonance imaging [16], field-cycling nuclear magnetic relaxometry in some ionomer membranes [17], *in situ* resistance measurements [18].

Unfortunately, all of them exhibit a rather low accuracy and/or spatial resolution. On the other hand, the most promising method, that is confocal micro-Raman spectroscopy [19], which combines high resolution with a good detection capability towards water, has been applied only to prototypes having some characteristics of fuel cells, but not to real working cells, yet.

An alternative approach based on the use of synchrotron radiation has been recently proposed [20]. In that paper, it is shown that X-ray diffraction is a suitable tool for *in situ* studies of this kind, since it is capable to reach high spatial resolutions (few microns of X-ray beam cross-sections) coupled with high signal to noise ratios.

* Corresponding author. Tel.: +39 0649934176; fax: +39 0649934153.
E-mail address: Alessandro.Isopo@artov.ism.cnr.it (A. Isopo).

0378-7753/$ – see front matter © 2008 Elsevier B.V. All rights reserved.
doi:10.1016/j.jpowsour.2008.06.046

In brief, the method consists of collecting a sequence of X-ray diffraction patterns taken from the membrane while the fuel cell is operating. The changes occurring in the pattern profile can be related to the variable contribution of water to the X-ray intensity diffracted by the hydrated membrane. A full description of the method can be found in Ref. [20].

In the present paper, we investigate the possibility to replace the synchrotron with a laboratory source, namely an ordinary X-ray tube. At a first glance, a X-ray tube might seem absolutely inadequate to carry out the same kind of diffraction studies, since its X-ray intensity is several orders of magnitude lower than that available at synchrotron facilities. As a consequence, the problems connected to its use might be considered insoluble. This is probably true for conventional X-ray diffraction (in the following referred to as angular dispersive, AD, technique), but not necessarily if the energy dispersive (ED) variant of X-ray diffraction is utilized. Indeed, the ED technique exhibits several merits with respect to its AD counterpart, some of which could allow performing the required measurements on proton exchange membranes (PEMs), as actually demonstrated by the final results of this paper.

The difference between the two alternatives AD/ED for X-ray diffraction can be explained through the definition of the scattering parameter q (amplitude of the momentum transferred from the photons to the sample electrons). Usually, a diffraction pattern is represented as the X-ray intensity diffracted by a sample versus the deflection angle 2ϑ. However, this definition is consistent only if the primary X-ray beam has a well-defined energy E. If E is varied, the pattern undergoes a non-linear stretching, that is to say, a compression, if E is increased, or an expansion, in the opposite case. If the pattern is plotted as a function of the scattering parameter q, instead of as a function of 2ϑ, a universal curve is obtained: any increase (decrease) of E will be counterbalanced by an opposite decrease (increase) of the diffraction angle 2ϑ, according to the following master equation: $q = aE \sin\vartheta$ (where a is constant equal to about 1.104 [Å keV]$^{-1}$) [21].

From such relation, it turns out that two alternative methods are available to scan the reciprocal space (the q-space), i.e. carrying out an angular scan by using a fixed-energy primary beam or, conversely, an energy scan at fixed angle. In the former case (AD), one makes use of a monochromatised primary beam and the angular scan is generally accomplished by progressively rotating the diffractometers arms; in the latter case (ED), the angle is unchanged during data collection and the E-scan is performed electronically by a suitable energy sensitive detector.

Although the ED exhibits a lower q-resolution than AD, it shows several merits that are fundamental in the present type of diffraction studies on fuel cells PEM. Indeed, from the experimental point of view, the lower q-resolution does not represent a major defect, since both the polymer membrane and the water contained in it, are non-crystalline specimens, thus characterised by broad peaks and diffused haloes. For this reason, a further slight broadening, induced by the low resolution of the detector, is not a problem. Vice versa, the high penetrating power of the upper energy components of the primary beam spectrum is an important merit, because it guarantees a sufficient transparency of the membrane even when the optical path is several centimeters long (that is the present case, as shown in the following Section 2).

In Fig. 1, the energy spectra of the X-ray radiation, before impinging on the membrane and after being transmitted through it, is plotted against the energy. It can be noticed that, below 25 keV, the signal is vanishingly small. Since the energies of the fluorescence lines, generally utilised as primary beams in laboratory AD, is below 22 keV, corresponding to the Ag Kα (while typically is about 8 keV, corresponding to the Cu Kα), the measurements could hardly be possible by using the AD mode.

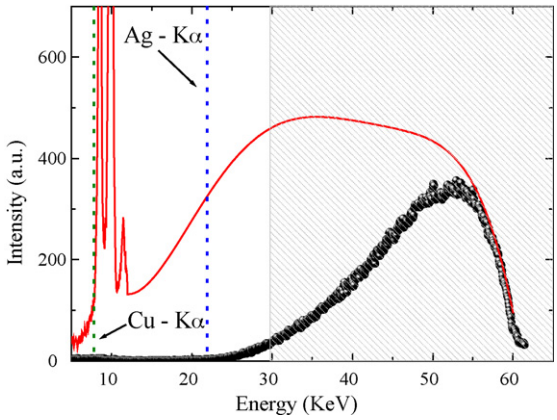

Fig. 1. Energy spectrum of the primary beam (red line) compared with the same beam after being transmitted through the membrane (black data points). The vertical dotted lines indicate, in green, the energy of the Cu Kα fluorescence line typically used in laboratory X-ray experiments (8.04 keV) and, in blue, the highest energy radiation among those produced by commercial X-ray tubes (Ag Kα at 22.11 keV). The grey sector on the right side of the graph, where the transmission is sufficiently high (from 10% at 30 keV, up to about unity above 55 keV), represents the energy range utilized in the present experiment. (For interpretation of the references to colour in this figure legend, the reader is referred to the web version of the article.)

Another important advantage is that in ED, unlike AD, both the experimental geometry and the portion of membrane sampled are unchanged during patterns collection. Therefore, membrane "slices" as thin as 20 μm (or even thinner) can be sampled, allowing the spatially resolved observation of their water content change.

2. Experimental

The ED diffractometer is equipped with a commercial W anode X-ray tube operating up to 60 kV and 25 mA. The collimation system is composed by three W slits adjustable, in our case, at steps of 20 μm. The cell is placed on a sample holder, in the centre of rotation of the arms. The holder can be translated vertically and tilted by remote controlled step motors. In this way, a precise cell positioning can be achieved and selected portions of the membrane can be sampled during the cell working.

To attain the spatial resolution required to observe the various slices in which the membrane can ideally be divided, the collimating slits must be set at their minimum aperture, namely 20 μm. In the present case, we make use of a Nafion 115 membrane, whose thickness is approximately 120 μm (see Fig. 2).

Neglecting the small beam divergence at the sample, the membrane can therefore be divided in six "slices" that can be observed independently. For doing this, the asymmetrical $(0, 2\vartheta)$ diffraction geometry must be utilised, since only this geometry assures the correct sampling of each single slice (Fig. 3A). Indeed, the symmetrical (ϑ, ϑ) geometry (usually preferred because requires simpler data corrections) would result in the irradiation of a rhomboidal-shaped volume, in which several adjacent layers contribute to the scattered intensity (Fig. 3B).

Of course, such a high spatial collimation is particularly detrimental for a laboratory source photon flux, because the intensity available for diffracting is proportional to the solid angle subtended by the slits apertures upstream of the sample. This further drawback must be added to the aforementioned weakness of polymers diffraction signals.

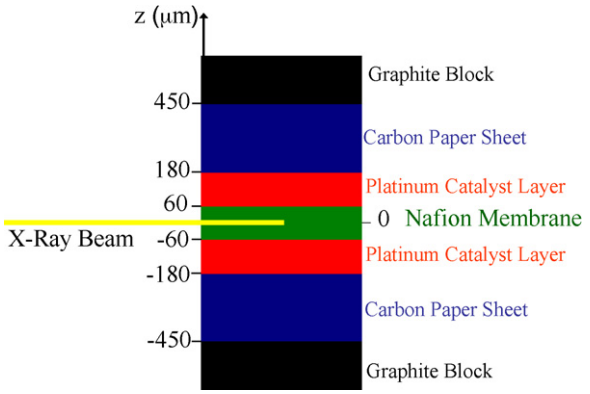

Fig. 2. Longitudinal view of fuel cell with respect to the incident X-ray beam direction. (For interpretation of the references to colour in this figure legend, the reader is referred to the web version of the article.)

Nevertheless, the characteristics of the ED X-ray diffraction discussed above (high penetration power of the primary X-ray beam and parallel collection of the energy components) largely balance these limitations. As a consequence, the collection times required to reach an acceptable signal to noise ratio, are "only" two orders of magnitude longer than at a synchrotron (say, several minutes instead of a few seconds). However, since the times required to reach equilibrium conditions are 1 h or even longer [19], very short acquisitions are unnecessary.

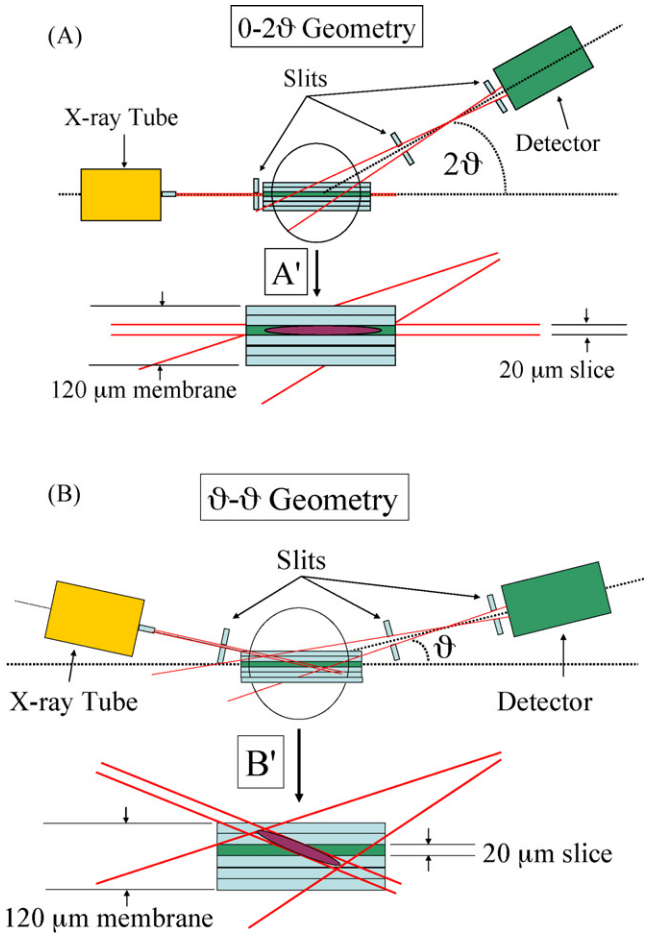

Fig. 3. (A) Asymmetrical (0–2ϑ) diffraction geometry adopted for these studies. In [A′] the membrane irradiation mode is highlighted. (B) Symmetrical (ϑ–ϑ) diffraction geometry. In [B′] the membrane irradiation mode is highlighted.

3. Results and discussion

3.1. Instrumental set-up

Prior to diffraction studies, an accurate experimental procedure is required to align and centre the membrane. Such procedure is aimed to place the membrane surfaces parallel to the primary X-ray beam (as in Fig. 3A) by tilting the cell and, then, to individuate its inner components (namely the membrane itself, the catalyst layers, the carbon paper sheets and the graphite blocks) by a vertical scan. The problem is that, in general, the primary beam will cross several components along its path inside the cell and, therefore, an experimental procedure to assure the parallelism is necessary. A suitable method to do this (with the help of the X-ray detector only) consists of collecting sequences of X-ray transmission spectra as follows. At first, the cell is placed in the centre of the diffractometer, paying attention to put the membrane as horizontal as possible by eye. Then, a vertical scan of the cell is carried out, acquiring a X-ray transmission spectrum at each step. In this way, the interfaces between the cell components are approximately found.

The alignment is then refined by repeating such procedure while progressively increasing the tilt angle α. In other words, a double scan of both the vertical coordinate z (at steps of 10 μm) and of the tilt angle α (at steps of 0.1°) is carried out, acquiring a transmission spectrum in correspondence of each couple of the parameters (z, α).

As an example, one of these sequences collected, at fixed α, as a function of z in the range (−0.3 to 0.3) mm, is shown in Fig. 4.

Integrating above the low energy region (where the signals get vanishingly small, say 30 keV) the X-ray transmission spectra collected at each α, the plots reported in Fig. 5A and B are obtained.

Comparing the curves in Fig. 5A and B, the tilt angle α that corresponds to parallelism between X-ray primary beam and the membrane surfaces is found and set to zero. Indeed, it can be readily identified as the one corresponding to the pattern that exhibits the sharpest edges at the interfaces and the widest central plateau (the plateau in the transmission spectrum corresponds to the zone of constant density, that is the membrane). The curve relative to $\alpha = 0$ is magnified in Fig. 6 to improve its visibility. Moving away from such α value in either direction, a progressive broadening of these edges, as well as a deformation of the membrane plateau, can be noticed. The edge broadening at $|\alpha| > 0$ testifies that the X-ray beam does not intercept a single layer only, but crosses transversally at least two adjacent layers (see the insets of Fig. 5, where the yellow

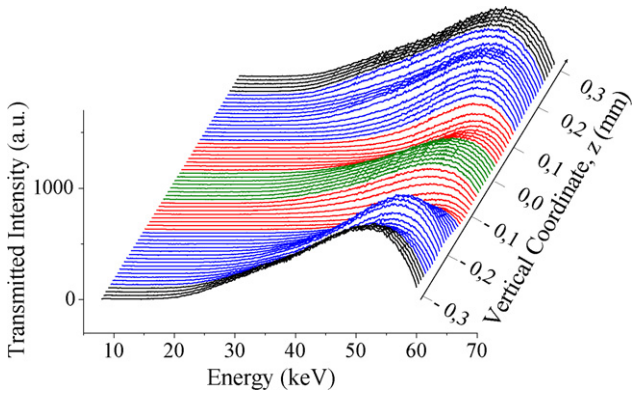

Fig. 4. Collection of X-ray spectra transmitted through the cell as a function of photon energy (keV) and the vertical coordinate z (mm) at fixed α. The same colours as Fig. 2 are used to distinguish the packets of transmission spectra through the various layers.

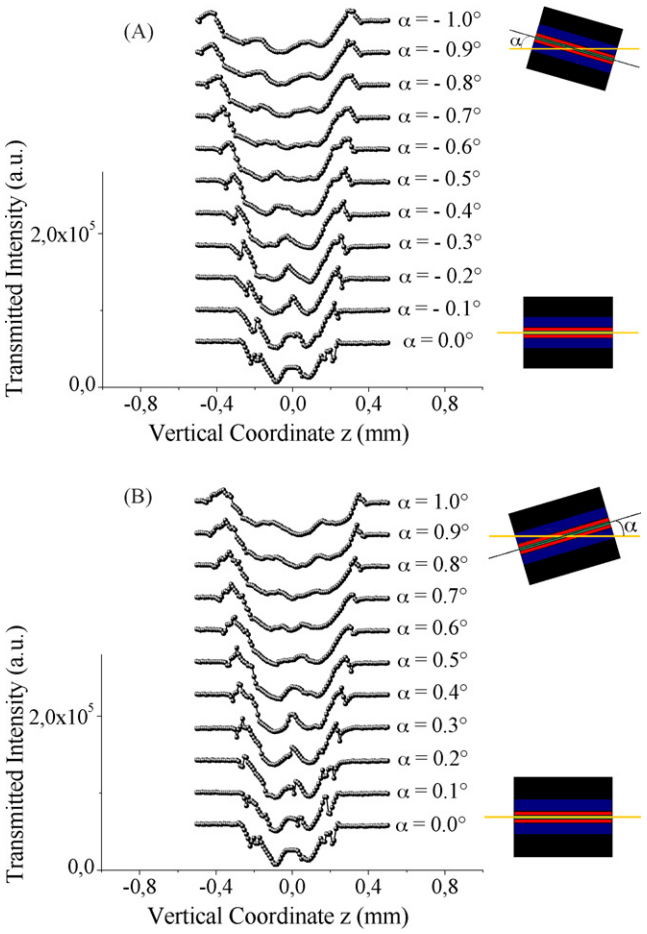

Fig. 5. (A) Transmission intensity integrated in the (30–60) keV range as function of the vertical coordinate z, at fixed (negative) values of the tilt angle α. (B) Transmission intensity integrated in the (30–60) keV range as function of the vertical coordinate z, at fixed (positive) values of the tilt angle α.

line represents the direction of the incoming X-ray beam). Indeed, a sudden change of the transmitted signal indicates the abrupt passage between materials having different absorption powers, while a smooth change indicates a progressive passage, that is to say, the presence of several materials along the X-ray path.

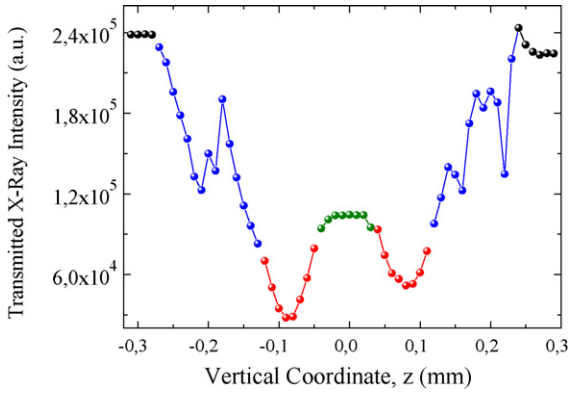

Fig. 6. Transmission intensity integrated in the (30–60) keV range as function of the vertical coordinate z, at $\alpha = 0$. The same colours as in Fig. 2 are used to distinguish data-points corresponding to the various layers (black for the graphite blocks, blue for the carbon paper sheets, red for the catalyst interfaces, green for the membrane). (For interpretation of the references to colour in this figure legend, the reader is referred to the web version of the article.)

The plot at $\alpha = 0$ in Fig. 6 shows clearly the identity of the various membrane electrode assembly (MEA) components.

Starting from the left side (black data-points), the first plateau corresponds to transmission through the inferior graphite block. The subsequent decrease (blue data-points) is due to the transmission through the carbon paper, more absorbing than the block. This can be justified taking into account that the reactant gases channels are grooved in the graphite cylinder at its interface with the carbon paper foil, thus reducing the average density of the material. Then, a peak is observed in this branch of the transmission curve. It can be attributed to the loose contact between the carbon paper and the Pt catalyst layer (red data-points), that is the most opaque material in the MEA. Finally, a new increase in the transmission leads to the central plateau of the plot, corresponding to the region of interest, i.e. the Nafion membrane (green data-points). The remaining part of the plot, on the right side, is approximately symmetrical to that just described.

3.2. EDXD measurements on the dry membrane

Once the sample has been aligned and the vertical intervals relative to the various layers of the MEA are identified, the sample is ready to be measured by X-ray diffraction.

However, according to the master equation $q = aE \sin\vartheta$, the q-values sampled at a given energy change with the angle. To get the maximum information, a diffraction pattern containing the major peaks of both water and Nafion in the high energy zone (to avoid the intensity decrease due to absorption) should be selected. For doing this, the optimal diffraction angle 2ϑ (see Fig. 3A) must be found. Therefore, leaving the X-ray tube arm in the horizontal position, the detector arm is progressively inclined (from $2\vartheta = 3^\circ$ to 8°, at steps of 1°), while a diffraction pattern is collected at each angular step, as shown in Fig. 7.

As discussed in Section 1, since the q-values at which the diffraction peaks are placed is fixed (being a structural property of the sample), the effect of an increase of 2ϑ is the shift of the peaks to lower energies, according to the previous master equation. Since lower energies correspond to higher opacity of the materials, the peak at $q = 1.16\,\text{Å}^{-1}$ (first diffraction peak of Nafion [20]), dominant at the lowest angle $2\vartheta = 3^\circ$, tends to rapidly disappear as ϑ is increased (Fig. 7). Conversely, a second diffraction peak at $q = 2.70\,\text{Å}^{-1}$ gets inside the accessible q-range at a higher angle ($2\vartheta = 7^\circ$), although its intensity is much lower. As a consequence of this test, we can conclude that a diffraction angle of $2\vartheta = 3^\circ$ is to be selected in the following *in situ* real-time measurements.

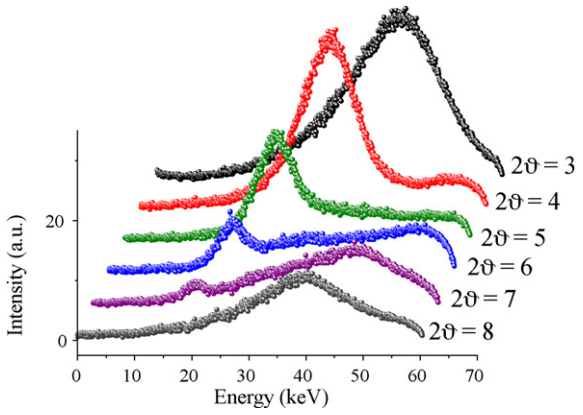

Fig. 7. ED X-ray diffraction patterns taken from a 20-μm slice of Nafion membrane at various diffraction angle 2ϑ, in the asymmetrical configuration [0–2ϑ]. To improve the visibility, the patterns are slightly offset along the energy axis.

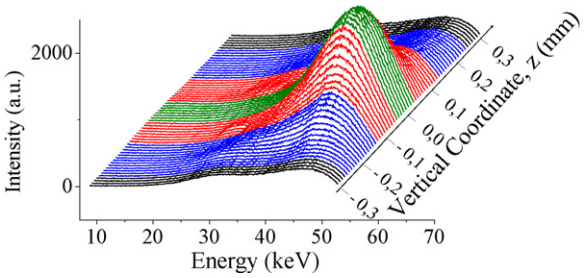

Fig. 8. Waterfall of ED X-ray diffraction patterns produced by the various layers of MEA, acquired in asymmetrical geometry [0–2ϑ], at fixed angle $2\vartheta = 3^\circ$. The same colours as in Figs. 2 and 4 are used to distinguish the layers.

The next step consisted of collecting a sequence of diffraction patterns upon a vertical scan analogous to that carried out in the transmission measurements shown in Fig. 4. In this way, the diffraction fingerprints of the various membrane "slices" could be detected (Fig. 8). From a direct comparison between such two figures, the consistency of the results obtained from the two kinds of measurements is evident. Indeed, as in the previous case of the transmission spectra, also in the sequence of diffraction patterns the components of the MEA can be readily distinguished and assigned to each layer (whose patterns are identified in Fig. 8 by the same colours used in Figs. 2 and 4).

3.3. Time-resolved ED X-ray diffraction study of the membrane water dynamics

Once both α and 2ϑ are selected in the way discussed above, a comparison between the diffraction patterns acquired on dry and on fully hydrated membrane (or, to be more precise, the minimum and maximum hydration degree of the membrane in the conditions reported below) can be made.

Accordingly, couples of patterns produced by the dry/fully hydrated membrane "slices" were collected as a function of the vertical coordinate. A selection of these couples is shown in Fig. 9.

In this experiment, the membrane is hydrated by direct wetting, namely filling the channels for the reactant gas injection with water, leaving the membrane in contact with water for about 20 h and, finally, removing the excess of water. The subsequent de-hydration is accomplished by fluxing N_2 in the same channels for about 5 h.

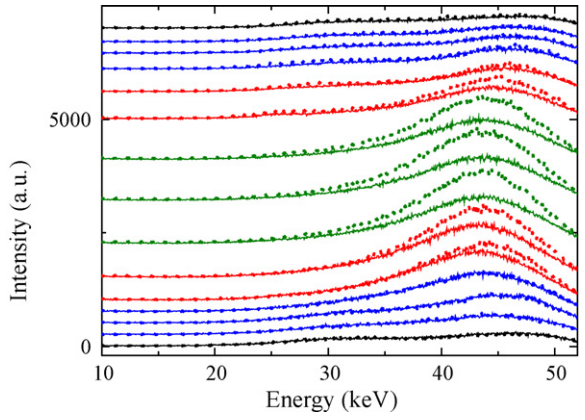

Fig. 9. Comparison among diffraction patterns of dry membrane (green dotted lines) and fully hydrated membrane (green solid lines). Diffraction patterns coming from the other layers are also reported, they are distinguished by colours as in Fig. 2. (For interpretation of the references to colour in this figure legend, the reader is referred to the web version of the article.)

As it can be noticed, the diffraction pattern corresponding to the "fully" hydrated condition is well distinguishable from the "dry" one, due to a variation of about one half in intensity of the peak at 43.7 keV (that corresponds to the first Nafion diffraction peak at $q = 1.16\ \text{Å}^{-1}$, according to the master equation calculated at $2\vartheta = 3^\circ$). This difference is constant, within the statistical uncertainty, for all the membrane slices. Indeed, as expected, in absence of the phenomena taking place when the cell is working, the membrane absorbs water uniformly.

Far from the membrane, the patterns (in black, corresponding to the graphite blocks) do not exhibit any change induced by hydration. However, slight differences due to presence of water in the vicinity of the membrane (i.e. in the catalyst layers and in the carbon paper sheets) not completely removed during the drying process, can be detected.

Focusing the attention on the membrane, it can be noticed that, when it is fully hydrated, a remarkable decrease of the Nafion first diffraction peak at $q = 1.16\ \text{Å}^{-1}$ is observed. Indeed, in this region, the water pattern [22,23] exhibits a minimum due to destructive interference among the waves scattered by its molecules. This decrease can be regarded as the fingerprint of water in the polymer network, so that the variation of the Nafion peak intensity can be directly correlated with the abundance of water in the (partially) hydrated membrane.

The algorithm to extract the information on the hydration degree from the diffraction patterns of a partially hydrated membranes has been described in the detail elsewhere [20].

In brief, this method consists of decomposing the diffraction pattern produced by the membrane at an intermediate hydration degree, as a combination of two reference functions that are the patterns of a dry and of a fully hydrated membrane, respectively. To clarify this procedure, a parallel can be made with what is usually done in quantum chemistry: in order to operate on the wavefunction of a quantum system in a mixed state, the wavefunction is decomposed ("projected") on the basis set of the Hamiltonian eigenfunctions (pure states) of the system itself. The coefficients so obtained represent the contribute of each pure state to the mixed state of the system. The same applies in the present case. The diffraction pattern of the partially hydrated state is decomposed on the base of the patterns representing the dry and the fully hydrated system.

Once the decomposition coefficients are obtained in this way, they are suitably weighted to take into account the specific scattering power of pure water, therefore providing the hydration degree required.

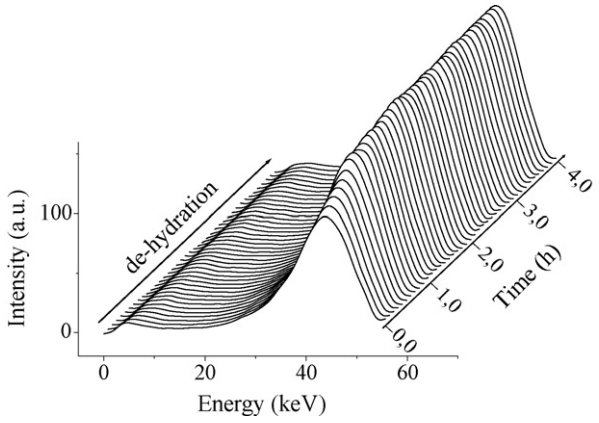

Fig. 10. Sequence of diffraction patterns corresponding to the drying of a single 20 μm slice of Nafion membrane.

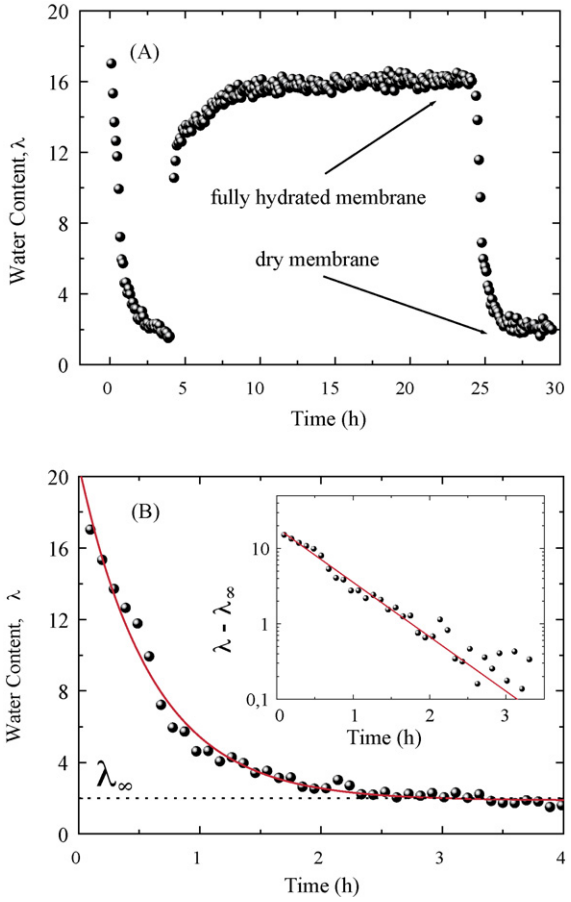

Fig. 11. (A) Water content determination in a complete de-hydration/hydration/de-hydration cycle of a single 20-μm slice of Nafion membrane as a function of time. (B) Evaluation of the characteristic time of the first de-hydration process. In this particular condition, it is of the order of 36 min.

In Fig. 10, the sequence of real-time diffraction patterns collected *in situ* upon de-hydration (namely, from the highest to the lowest hydration degree consistent with our experimental conditions) of the 20 μm thick central slice of the membrane is shown. The value of 20 μm represents the space resolution of these measurements.

In Fig. 11A, the water content of the membrane central slice upon a de-hydration/hydration/de-hydration cycle is plotted in terms of the λ parameter vs. time, where λ is the number of water molecules per sulfonic acid group [24]. Although the vertical width of the primary X-ray beam is only 20 μm and the diffraction patterns are collected for about 5 min each, the intensity is sufficient to plot a curve with a low scattering of data-points and with a good reproducibility.

In Fig. 11B, an exponential decay fit of the first de-hydration curve is shown. The agreement between data-points and theoretical curve can be more clearly appreciated in the semi-log plot reported in the inset. The characteristic time of the process is consistent with the previous experiment accomplished at the synchrotron facility [20], the small discrepancy being attributable to the slightly different experimental conditions.

4. Conclusions

An experimental procedure to carry out laboratory X-ray diffraction investigation to observe real-time changes of the water content of a fuel cell PEM has been discussed.

It is shown that the severe limitations coming from the low energy and low intensity of laboratory sources can be partly overcome by means of the energy dispersive method, if preliminary procedures to align and centre the cell have been correctly carried out. The measurements discussed in this paper have been performed on a non-operating fuel cell, the membrane hydration and subsequent de-hydration being accomplished by direct wetting and drying. However, since such diffraction technique is sensitive to the water amount present in the portion of membrane sampled, regardless of the way the water got inside the membrane, the method can be straightforwardly applied to operating fuel cells. This provides a new non-destructive tool for space/time-resolved investigations of the water management in PEMs of fuel cell upon working.

Acknowledgement

This research has been carried out within the NUME Project "Development of composite proton membranes and of innovative electrode configurations for polymer electrolyte fuel Cells", financially supported by the Italian Ministry of University and Research (FISR 2003).

References

[1] K.A. Mauritz, R.B. Moore, Chem. Rev. 104 (2004) 4535–4585.
[2] W.Y. Hsu, T.D. Gierke, J. Membr. Sci. 13 (1983) 307–326.
[3] H.L. Yeager, A. Steck, J. Electrochem. Soc. 128 (1981) 1880–1884.
[4] M.K. Petersen, F. Wang, N.P. Blake, H. Metiu, G.A. Voth, J. Phys. Chem. B 109 (2005) 3727–3730.
[5] T.A. Zawodzinski, C. Derouin, S. Radzinski, R.J. Sherman, V.T. Smith, T.E. Springer, S. Gottesfeld, J. Electrochem. Soc. 140 (1993) 1041–1047.
[6] M. Ise, K.D. Kreuer, J. Maier, Solid State Ionics 125 (1999) 213–223.
[7] S. Ge, X. Li, B. Yi, I.-M. Hsing, J. Electrochem. Soc. 152 (2005) 1149–1157.
[8] T.E. Springer, T.A. Zawodzinski, S. Gottesfed, J. Electrochem. Soc. 138 (1991) 2334–2342.
[9] D.M. Bernardi, M. Verbrugge, J. Electrochem. Soc. 139 (1992) 2477–2491.
[10] T.E. Springer, M.S. Wilson, S. Gottesfeld, J. Electrochem. Soc. 140 (1993) 3513–3526.
[11] M. Eikerling, Y.I. Kharkats, A.A. Kornyshev, Y.M. Volfkovich, J. Electrochem. Soc. 145 (1998) 2684–2699.
[12] R.J. Bellows, M.Y. Lin, M. Arif, A.K. Thompson, D. Jacobson, J. Electrochem. Soc. 146 (1999) 1099–1103.
[13] R. Satija, D.L. Jacobson, M. Arif, S.A. Werner, J. Power Sources 129 (2004) 238–245.
[14] J. Zhang, D. Kramer, R. Shimoi, Y. Ono, E. Lehmann, A. Wokaun, K. Shinohara, G. Scherer, Electrochim. Acta 51 (2006) 2715–2727.
[15] R. Mosdale, G. Gebel, M. Pineri, J. Membr. Sci. 118 (1996) 269–277.
[16] S. Tsushima, K. Teranishi, S. Hirai, Energy 30 (2005) 235–245.
[17] J.C. Perrin, S. Lyonnard, A. Guillermo, P. Levitz, J. Phys. Chem. B 110 (2006) 5439–5444.
[18] F.N. Buchi, G.G. Scherer, J. Electrochem. Soc. 148 (2001) 183–188.
[19] H. Matic, A. Lundblad, G. Lindbergh, P. Jacobsson, Electrochem. Solid State Lett. 8 (2005) 5–7.
[20] V. Rossi Albertini, B. Paci, A. Generosi, S. Panero, M.A. Navarra, M. di Michiel, Electrochem. Solid State Lett. 7 (2004) 519–521.
[21] R. Caminiti, V. Rossi Albertini, Int. Rev. Phys. Chem. 18 (1999) 263–299.
[22] A.H. Narten, M.D. Danford, H.A. Levy, Discuss. Faraday Soc. 43 (1967) 97–107.
[23] K. Nishikawa, N. Kitagawa, Bull. Chem. Soc. Jpn. 53 (1980) 2804–2808.
[24] A.Z. Weber, J. Newman, J. Electrochem. Soc. 150 (2003) 1008–1015.